Particle Astrophysics

Second Edition

D. H. PERKINS

Particle and Astrophysics Department
Oxford University

OXFORD
UNIVERSITY PRESS

7 Dark matter and dark energy components

7.1 Preamble

In Chapter 5 we already noted that it appears that a large fraction of the matter in the universe is dark (i.e. non-luminous) matter. The need to postulate such dark matter was noted as early as the 1930s by Zwicky, who observed that galaxies in the Coma cluster seemed to be moving too rapidly to be held together by the gravitational attraction of the visible matter. Obviously, we can hardly be satisfied with our picture of the universe until the nature and distribution of such vast quantities of matter has been settled. For example, an important question is whether this dark matter is in the form of new types of (stable) elementary particle, which have been roaming around since the earliest stages of the Big Bang: and if so, what are such particles, and why have we not met with them in accelerator experiments? Or, could it be that some of the dark matter is agglomerated in the form of non-luminous stellar objects made out of the same matter as ordinary stars, or as mini black holes or whatever?

According to present ideas, the quark and lepton constituents of matter with which we are familiar in experiments at accelerators, produced in the numbers foreseen by the model of nucleosynthesis in the early universe described in Chapter 6, can account for only about 4% of the present energy density of the universe. Dark matter is estimated to account for some 20% of the total energy density, but the bulk of the energy density—that is, some 76%—has to be assigned to 'dark energy', which in Chapter 5 was identified with vacuum energy. However, the true source of the dark energy—like that of the dark matter—is unknown at present.

Before proceeding further, we should recall that, of the total baryonic contribution deduced from primordial nucleosynthesis as described in Chapter 6, only about 10% is accounted for by the luminous matter in stars and galaxies. Hot gas in galaxy clusters and intergalactic hydrogen accounts for a further 40%, leaving half the baryons unaccounted for. As described in Section 7.5, some baryons are located in dark, compact stellar-like objects (MACHOs, or massive astrophysical compact halo objects) in galactic halos, detected by their gravitational lensing of light signals from more distant stars. However, these can account for only a small part of the baryon contribution. Recent observations, discussed in Section 7.7, indicate that the missing baryonic matter may be associated with blazers (see Section 9.14.2).

In this chapter, we first present the evidence for the existence of dark matter, then describe briefly some of the possible dark matter candidates and the attempts to detect them directly. Finally, we describe the evidence

for the acceleration of the Hubble expansion from the study of high redshift supernovae, and the consequences for the dark energy/cosmological constant.

7.2 Dark matter in galaxies and clusters

The classical evidence for dark matter comes from the measurement of the rotation curves of velocity versus radial distance for stars and gas in spiral galaxies. This has given strong, if indirect, indications for the existence of 'missing' mass, in the form of non-luminous matter. Consider, for example, a star of mass m at distance r from the galactic centre, moving with tangential velocity v as shown in Fig. 7.1. Then equating gravitational and centrifugal forces we obtain

$$\frac{mv^2}{r} = \frac{mM\,(<r)\,\mathrm{G}}{r^2} \tag{7.1}$$

where $M(<r)$ is the mass inside radius r. A spiral galaxy such as our own has most of the luminous material concentrated in a central hub plus a thin disc. For a star inside the hub, we expect $M(<r) \propto r^3$ and therefore $v \propto r$, while for one located outside the hub, $M \sim$ constant and therefore we expect $v \propto r^{-1/2}$. Hence, the velocity should increase at small r and decrease at large r. On the contrary, for many spiral galaxies, the rotation curves are quite flat at large r values. An example is shown in Fig. 7.2. This has led to the suggestion that the bulk of the galactic mass—typically 80–90%—is in the form of dark matter in a halo as in Fig. 7.1.

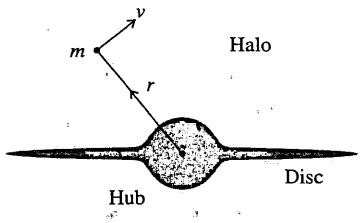

Fig. 7.1 An end-on view of a spiral galaxy, consisting of a central hub, a disc, and a possible halo of dark matter.

Surveys of galaxy clusters show that much of the 'visible' mass is in the form of very hot, X-ray emitting gas. The gas temperature (typically 10^7 to 10^8 K) estimated from the X-rays measured with the ROSAT satellite implied velocities of gas particles far in excess of the escape velocities as deduced from the visible mass. If the gas is bound by gravitational forces, suggested by the fact that it appears concentrated towards the cluster centres, the greater part (at least 80%) of the total mass must be dark matter.

The major surveys of galaxies and galaxy clusters, such as the infrared IRAS satellite survey, comparing the motional energy with the gravitational energy, also provide evidence for dark matter. This analysis is based on the *virial theorem* of classical mechanics. This relates the time average of the potential energy $<V>$ to that of the kinetic energy $<E>$ of a bound system of i non-relativistic particles of masses m_i, velocities $\mathbf{v}_i$, momenta $\mathbf{p}_i$, and kinetic energies E_i, interacting *via* a central inverse square law of force, $\mathbf{F}_i$. The virial is defined as $W = \Sigma \mathbf{p}_i \cdot \mathbf{r}_i$, where $\mathbf{r}_i$ is a position vector measured from some arbitrary origin. On differentiation with respect to time this becomes

$$\begin{aligned}\frac{\mathrm{d}W}{\mathrm{d}t} &= \sum \dot{\mathbf{p}}_i \cdot \mathbf{r}_i + \sum \mathbf{p}_i \cdot \dot{\mathbf{r}}_i = \sum m_i \ddot{\mathbf{r}}_i \cdot \mathbf{r}_i + \sum m_i |\mathbf{v}_i|^2 \\ &= \sum \mathbf{F}_i \cdot \mathbf{r}_i + 2\sum E_i = \sum \left(\frac{\partial V_i}{\partial r_i}\right) \cdot \mathbf{r}_i + 2\sum E_i \\ &= -\sum V_i + 2\sum E_i\end{aligned}$$

where in the last line we have used the fact that the gravitational potential varies as $1/r$. Averaged over a time interval T, the virial of a *bound* system

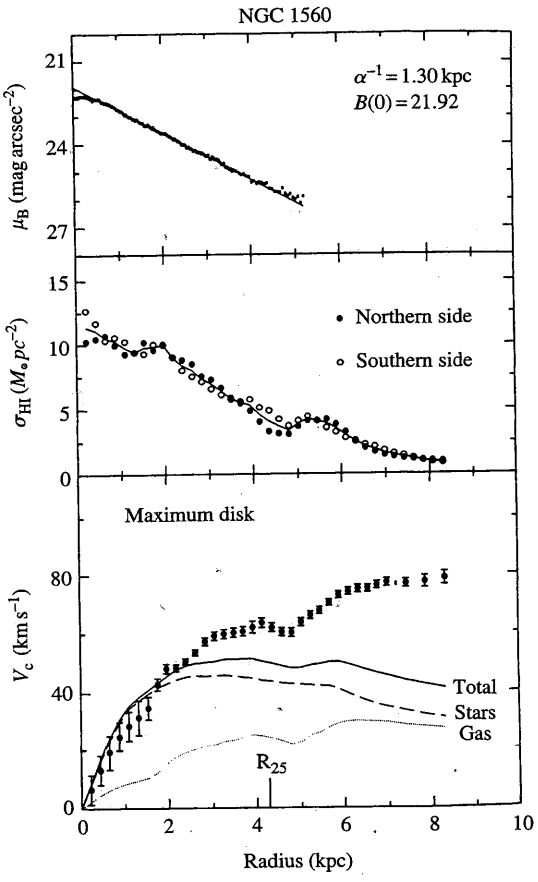

Fig. 7.2 Example of rotation curves for the spiral galaxy NGC 1560. In the top panel the luminosity is plotted against radial distance, showing an exponential fall-off. The middle panel shows the luminosity in the $H\alpha$ line. In the bottom panel, the points show the observed tangential velocities of stars in this galaxy as a function of radial distance. The curves show the expected values obtained by numerical integration of the mass inside a particular radius as in (7.1), with the contributions from stars and gas shown separately. They are clearly unable to account for the observed velocities at large radii (from Broeils 1992).

$\langle W \rangle = (1/T) \int (dW/dt)\, dt \to 0$ as $T \to \infty$, so that the time-averaged $\langle V \rangle = 2 \langle E \rangle$.

Measurements have been made with the Chandra satellite experiment (Allen *et al.* 2004) recording X-rays from large galaxy clusters, which contain many hundreds of galaxies embedded in them. As they are the largest bound systems known, the assumption made is that they represent a fair sample of the material of the entire universe. The clusters contain X-ray emitting gas at temperatures of order 10^6 K, and the virial theorem shows that dark matter is required to hold the clusters together. The X-ray observations actually allow one to estimate the ratio of the mass of hot gas to dark matter in a cluster. Making the reasonable assumption that this ratio is the same for all clusters, one can adjust the distance scale and hence absolute luminosity for each cluster to get the best fit to a universal value of the gas to dark matter ratio. In this way it could also be shown that the early deceleration of the expanding universe, due to the gravitational attraction of matter, was replaced by acceleration about 6 billion years ago. These results agreed perfectly with earlier, independent measurements, that dark energy accounts for 76%, dark matter for 20%, and baryonic matter for 4% of the energy of the universe. These previous observations came from high redshift supernovae, discussed later in this chapter (Section 7.14). It is in fact

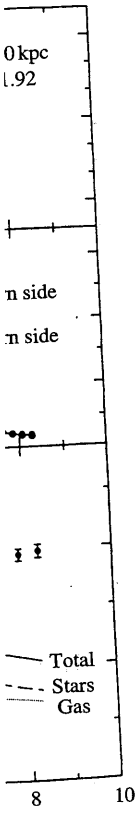

remarkable and heartening that quite different techniques for estimating the basic parameters of the universe are in such good agreement.

Some of the most remarkable evidence for dark matter comes from the observation of emission lines from very distant clouds of hydrogen, indicating redshifts of $z = 5$ or 6, located in vast galaxies of what appears to be dark matter, accounting for at least 99% of the total mass. Dark matter seems also to be required from quite independent considerations of the level of fluctuations in the cosmic microwave background and the growth of structure in the early universe, as discussed in Chapter 8. These density fluctuations are observed to be of order $\Delta\rho/\rho \sim 10^{-5}$, and fluctuations 2–3 orders of magnitude larger would have been necessary if formation of galaxy and galaxy clusters was to be achieved by gravitational collapse of baryonic matter alone, once it had decoupled from radiation at $z \sim 1000$. On the other hand, as discussed in Section 5.13, the existence of (cold) dark matter with $\Omega_{\rm cdm} \sim 0.20$ would have led to dominance of matter over radiation at a higher redshift ($z \sim 3000$) and more effective gravitational collapse of matter (with the gravitational field of the dark matter dragging baryonic matter along with it) from a much earlier epoch.

Finally, the masses of galaxy clusters and the contribution of dark matter can be estimated directly by their effects on the images of more distant quasars, due to the process of gravitational lensing, which is discussed in the following sections. It has the advantage that it avoids some of the assumptions necessary for other methods.

7.3 Gravitational lensing

Very important information regarding the amount and location of dark matter has come from gravitational lensing, which we therefore discuss at some length. The gravitational deflection of photons passing by a point mass M at a distance of closest approach b was given in Section 2.6 by the formula (2.28):

$$\alpha = \frac{4GM}{c^2 b} \tag{7.2}$$

This is the deflection predicted by Einstein's general theory of relativity, being exactly a factor 2 larger than the deflection one obtains according to Newtonian mechanics (see Problem 7.1). The correctness of the Einstein prediction was first demonstrated by the 1919 solar eclipse expedition by Eddington to the island of Principe, which measured the deflection of light from stars close to the Sun's limb.

The gravitational deflection of light implies that massive objects may act as *gravitational lenses*, as foreseen by Einstein even before the relation (7.2) had been tested experimentally. Suppose in Fig. 7.3 that S is a source of light (star) and that the rays to the observer O pass close to a massive point lensing object L of mass M. The diagram represents the situation in the plane defined by O, S and L, and is the gravitational analogue of a thin lens system in optics. In the general case, the source and lens will not be collinear with the observer and there will then be two images of the source, S1 and S2. Then if α denotes

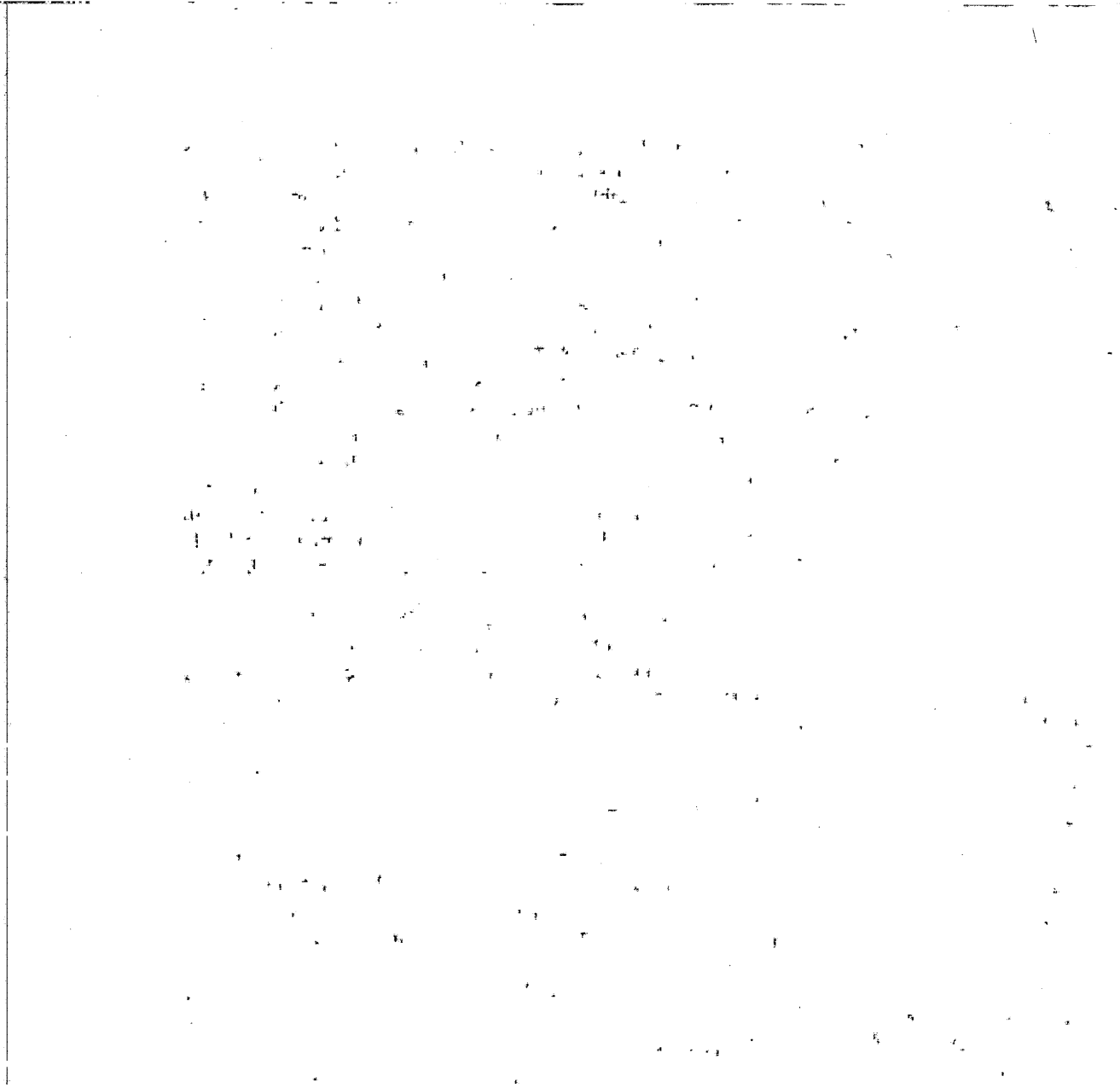

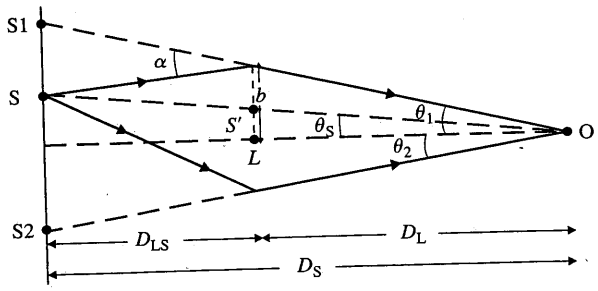

Fig. 7.3 The two images S1 and S2 of a source S formed from gravitational lensing by the point mass L.

the gravitational deflection and b the closest distance of approach, we have from (7.2):

$$\alpha D_{LS} = D_S(\theta_1 - \theta_S)$$

$$\theta_S = \theta_1 - \left(\frac{4GM}{bc^2}\right)\left(\frac{D_{LS}}{D_S}\right) = \theta_1 - \left(\frac{4GM}{c^2}\right)\left(\frac{D_{LS}}{D_S D_L}\right)\left(\frac{1}{\theta_1}\right) \quad (7.3)$$

In the collinear case, $\theta_S = 0$. Then we can write

$$\theta_1 = \theta_E = \left[\left(\frac{4GM}{c^2}\right)\left(\frac{D_{LS}}{D_S D_L}\right)\right]^{1/2} \quad (7.4)$$

where θ_E is the angle of the so-called *Einstein ring*. In this collinear case, the image of S is a ring of light centred on the line of sight. For finite θ_S and a point lensing mass, however, one obtains just two images lying in the plane defined by the source, lens, and observer, with angles which are solutions of the quadratic (7.3):

$$\theta_{1,2} = \left[\theta_S \pm \sqrt{\theta_S^2 + 4\theta_E^2}\right] \quad (7.5)$$

7.4 Evidence for dark matter from gravitational lensing

The above analysis assumed a point lensing mass. Often, the lensing object or objects will be extended in space, and more complex, multiple images are then formed. Examples of lensing were first observed for very intense and very distant sources called quasi-stellar radio sources or *quasars*, which are in fact the most powerful radio and optical sources known (see Section 9.14). Quasars are examples of galaxies with very active galactic nuclei (AGNs), and are almost certainly powered by the gravitational energy from massive black holes (see Section 9.15). In the case of quasars the lensing mass is a 'foreground' galaxy or galaxy cluster. An early example of a doubly imaged quasar is shown in Fig. 7.4.

When the lensing galaxies or clusters are extended objects, the lensed images of more distant objects can appear as multiple arcs, as shown in Fig. 7.5. Since in multiply imaged events, the different images involve different light paths, time

Relative flux

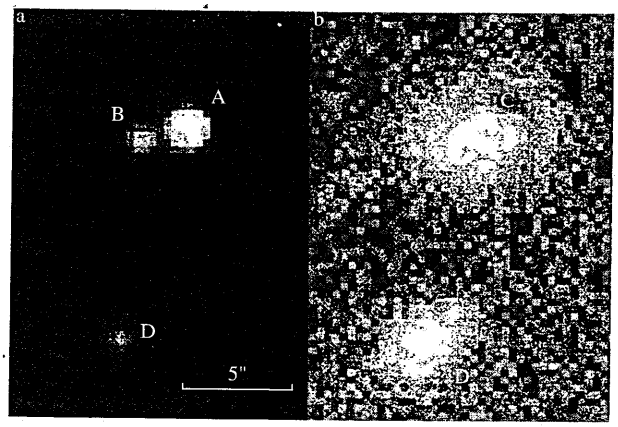

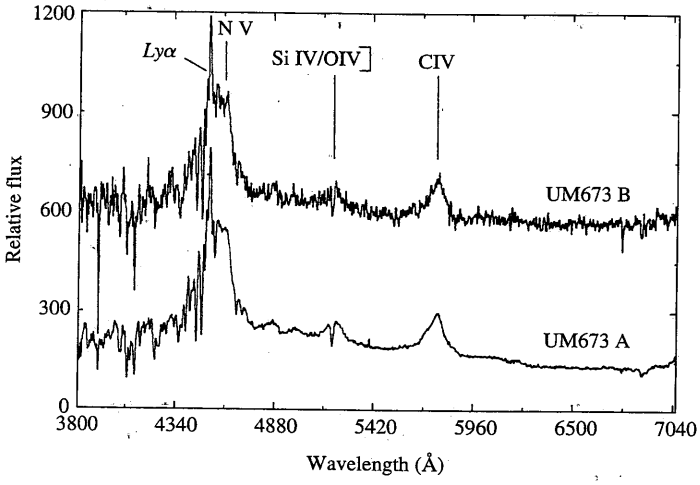

Fig. 7.4 An example of the double image of a quasar, observed by the European Southern Observatory, as it is lensed by a foreground galaxy. The top picture shows (at left) the quasar CCD image split into two parts, A and B. Subtracting these images from the frame reveals (at right) the lensing galaxy marked C. Object D is a background galaxy. The plot of the wavelength response at bottom shows that the two images, separated by 2.2 s of arc, have identical spectra (from Surdej *et al.* 1987).

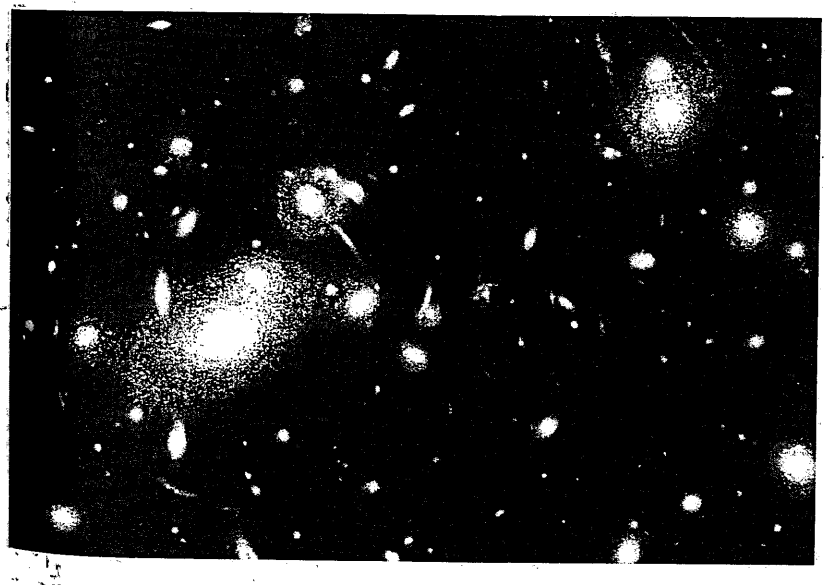

Fig. 7.5 Multiple images, seen in the form of long faint arcs, due to lensing effects by the galaxy cluster Abell 2218 of more distant galaxies. Picture by Hubble Space Telescope (Kneib *et al.* 1996).

delays will be involved. The path lengths are proportional to the distance scale, that is, to the inverse $1/H_0$ of the Hubble parameter, so that study of multiply-imaged quasars offers a method to determine H_0. However, the important thing is that by measurement of the multiple images of such distant quasars, the total gravitating mass of the foreground galaxy or cluster can be measured. The total mass density of the universe found in this way also indicates a value for the closure parameter associated with the matter content of $\Omega_m \approx 0.24$, as quoted in (5.33).

An example of the power of the lensing technique in providing quite compelling evidence for dark matter is provided by observations (Clowe *et al.* 2006) made using a combination of the Hubble Space Telescope, the ESO Very Large Telescope, the Magellan telescope, and the Chandra X-ray satellite. They observed a system of two galaxy clusters apparently having passed through each other. Using gravitational lensing of more distant galaxies by this cluster, it was possible to map the gravitational potential in the cluster, and thus the total matter distribution. On the other hand, the X-ray signals indicate the distribution of hot gas (i.e. the plasma of baryonic matter), and of course the luminous matter in stars is observed by the optical telescopes. The dark matter appeared in two distinctly separated regions. The X-rays were also found to be located in two regions, which are, however, well separated from the dark matter regions (see Fig. 7.6). The importance of these observations is that the regions of dark matter and of baryonic matter are distinct and well separated. In such a collision, as the two clusters pass through each other, the gas clouds would be slowed through electromagnetic interactions, but not the dark matter clouds, presumably subject only to the weak and gravitational interactions. Because of this spatial separation of dark matter and of baryonic matter, the observations cannot be explained as an artefact, due, for example, to a modification of the law of Newtonian gravity at large distances.

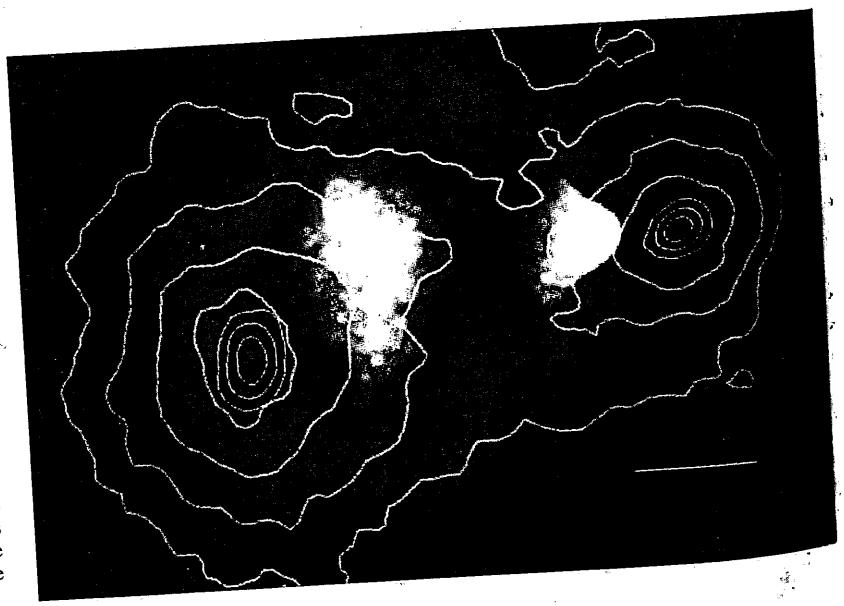

Fig. 7.6 The galaxy cluster 1EO657-558 observed by Clowe *et al.* (2006), interpreted as a case of two clusters passing through each other. The two white areas show the sources of X-rays measured by the Chandra satellite, and correspond to the regions of hot plasma (baryonic matter). The contour lines indicate the regions of dark matter deduced from the gravitational lensing of background galaxies (observed with optical telescopes) and these are seen to be distinctly separated from the plasma regions.

7.5 Amplification by gravitational lenses: microlensing and MACHOs

While gravitational lensing is commonly observed for massive lensing objects such as galaxies and clusters, distinct and separated images are not produced by individual stars, as the resolution of the best optical telescopes is simply not good enough, as shown in Example 7.1 below. While objects of typical stellar masses are too close to be resolved, distinguishing separate images is clearly possible for massive lensing objects, that is, for galaxies or galaxy clusters. Consider, for example, a cluster of mass $10^{14}M_{\rm sun}$, with $D_{\rm LS} = D_{\rm L} = D_{\rm S}/2 = 100\,$Mpc. Then $\theta_{\rm E} \sim 65\,$arc sec (assuming one can treat the cluster as a point mass), which is quite measurable.

Example 7.1 *Estimate the value of the Einstein radius for lensing by a stellar-type mass in the local galaxy, by considering the specific case of a pointlike lensing object of 10 solar masses, situated midway between the observer and a source at distance 2 pc (6×10^{16}m)—a typical interstellar distance. In this way discuss the possibility of observing separated images of individual stars with optical telescopes.*

Inserting the above numbers in (7.4), the value of the Einstein radius is found to be $\theta_{\rm E} = 0.32\mu{\rm rad} = 0.065\,$arc sec. One has to compare this angle with the resolving limit of a telescope. An earth-bound optical telescope has a resolution of about 1 arc sec (5μ rad), and even that of the Hubble Space Telescope is good to only 0.1 arc sec. So, resolving separate optical images of sources lensed by objects of stellar mass is not feasible.

Even when the images of a source produced by gravitational lensing cannot be resolved, an amplification of the intensity may occur, in what is called a *microlensing event*. Suppose that a pointlike lensing mass is moving at velocity v normal to the line of sight, and that the source subtends an angle $\theta_{\rm S}$ at the observer. All quantities are measured in the plane defined by the observer, lens, and source, with the notation of Fig. 7.3. In this case the angle $\theta_{\rm S}$ will be a function of time, with a minimum value when the lens is at the closest distance of approach to the line of sight to the source. From Fig. 7.7, the right-angled triangle AS′L gives us $\mathrm{LS}'^2 = \mathrm{AS}'^2 + \mathrm{AL}^2$, where $\mathrm{LS}' = D_{\rm L}\theta_{\rm s}$, $\mathrm{AS}' = D_{\rm L}\theta_{\rm s}({\rm min})$, and $\mathrm{AL} = vt$, where time t is measured from the moment of closest approach of the lensing object to the line of sight to the source. Dividing through by $(D_{\rm L}\theta_{\rm E})^2$ and with $x = \theta_{\rm S}/\theta_{\rm E}$, $x\,({\rm min}) = \theta_{\rm S}\,({\rm min})/\theta_{\rm E}$, we obtain

$$x^2 = x^2\,({\rm min}) + \left(\frac{vt}{D_{\rm L}\theta_{\rm E}}\right)^2 = x^2\,({\rm min}) + \frac{t^2}{T^2} \tag{7.6}$$

where in the second line we have defined $T = D_{\rm L}\theta_{\rm E}/v$. When the two images are not separated, there results an amplification of the (single) signal. From Liouville's theorem, the phase–space density, that is, the number of photons per unit solid angle, is unaffected by the imaging, so that if θ is the angle of the image, the amplification will be the ratio of solid angles, or

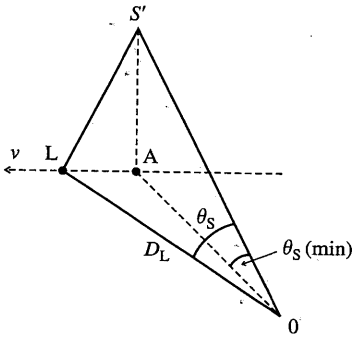

Fig. 7.7 A point lensing mass L moving with velocity v perpendicular to the line of sight. O is the observer and S′ is the projected position of the source in the plane of the lens.

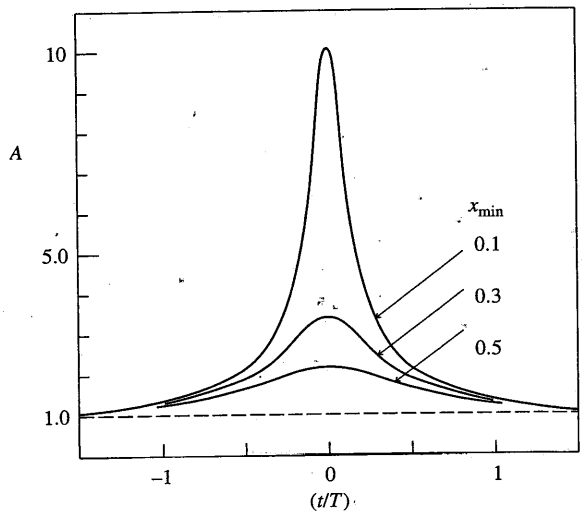

Fig. 7.8 Examples of the dependence of the amplification for microlensing events calculated from (7.8) for different values of x(min) as a function of t/T.

$A = \mathrm{d}\Omega/\mathrm{d}\Omega_S = \theta\,\mathrm{d}\theta/\theta_S\,\mathrm{d}\theta_S$. Since from (7.5)

$$\frac{\theta}{\theta_S} = \left(\frac{1}{2x}\right)\left[1 + \left(\frac{2}{x^2}\right) \pm x\sqrt{1 + \frac{4}{x^2}}\right] \tag{7.7}$$

it follows that, adding the amplitudes from the two (unresolved) images, the net amplification becomes

$$A = \frac{(1 + x^2/2)}{\left[x\sqrt{1 + x^2/4}\right]} \tag{7.8}$$

with x^2 defined in (7.6). Figure 7.8 shows how the signal depends on time, for a few cases of the ratio x(min). For $x(\mathrm{min}) \ll 1$, the peak value of A is approximately equal to $1/x\,(\mathrm{min})$. Figure 7.9 shows an example of a microlensing event, in which a massive dark object amplifies the light signal from a star in the Large Magellanic Cloud (a nearby mini-galaxy).

Example 7.2 *Calculate the typical time T for lensing by a pointlike object of mass 0.1 M_{sun}, moving at a velocity of $v = 200\,km\,s^{-1}$ normal to the line of sight, and situated half way to a source star at a distance of 50 kpc.*

Inserting these numbers in the above equations gives $\theta_E = [(4GM/c^2)\,(D_{LS}/D_S D_L)]^{1/2} = 6.2 \times 10^{-10}$ rdn and $T = D_L\theta_E/v = 2.39 \times 10^6$ s $\sim$ 28 days.

MACHOs is the name given to dark matter in the form of microlensing objects with masses of the order of stellar masses, in our galaxy. Typically their masses lie in the range 0.001–0.1 solar masses. Several hundred MACHOs have been observed, for example, by their microlensing of light from stars in the Large Magellanic Cloud, as in Fig. 7.9. A characteristic of these events is that the same amplification is observed in blue and red light, a fact which distinguishes them from variable stars. The reason for the achromaticity is clear. If the photon momentum is p, its effective gravitational mass is p/c, so that it will receive a

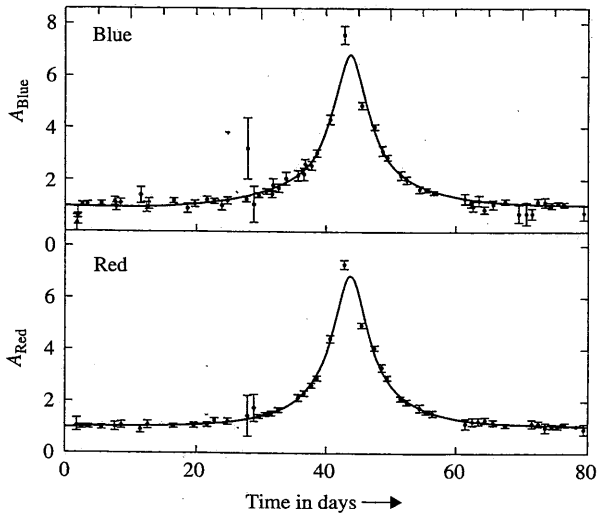

Fig. 7.9 Example of a microlensing event, the source being a star in the Large Magellanic Cloud, at a distance of some 50 kpc. Note the same signal is observed in blue and in red light. (After Alcock *et al.* 1993.)

transverse momentum $\Delta p \propto p$ from a gravitational field. Hence the deflection $\Delta p/p$ will be independent of wavelength h/p.

7.6 The lensing probability: optical depth

The probability that a particular source will undergo gravitational lensing as a measurable effect is called the *optical depth*. This is defined as the probability that at some instant of time, the line of sight to an individual star will be within the Einstein radius of a lens in the intervening distance. If N_L is the density of lenses per unit volume, and they are distributed uniformly, then since an Einstein ring extends over an area of $\pi(D_L\theta_E)^2$ it follows that the optical depth will be

$$\tau = \int \pi D_L^2 N_L \, dD_L \cdot \theta_E^2$$

where the integral extends from $D_L = 0$ to $D_L = D_S$. Substituting for θ_E from (7.4) and with $y = D_L/D_S$ and $\rho = N_L M$ for the mass density of lenses, the integral becomes

$$\tau = 4\pi G \left(\frac{D_S}{c}\right)^2 \int \rho(y) \cdot y \cdot (1-y) \, dy$$

with y running from 0 to 1. If ρ is constant, this expression simplifies to

$$\tau = 2\pi G \left(\frac{D_S}{c}\right)^2 \frac{\rho}{3} \tag{7.9}$$

which depends only on the distance to the source and the average mass density of lensing objects between the observer and the source. Inserting typical values of density for our galaxy, and considering sources near the periphery of the central bulge at ~ 5 kpc, yields a value of $\tau \sim 10^{-7}$. Thus lensing will be

a comparatively rare occurrence, and to detect dark matter in the form of 'dark stars'—that is, MACHOs as described above—one needs to examine the light curves of many millions of stars over months and years. This has required computerized search techniques, of the type first used in the old automated analysis systems in scanning bubble chamber film in particle physics experiments.

The magnitude of the magnification involved in microlensing varies inversely as the impact parameter between the lensed star and the MACHO, and so detection of microlensing typically involves examination of millions of stars, as discussed above. On the other hand, the Shapiro time delay falls off only logarithmically with impact parameter, so even with only a few thousand known pulsars, an effect may be detectable, although so far none has been claimed.

The present evidence is that MACHOs appear to account for only a small fraction of all the baryonic matter. The majority is in the form of stars, gas, and dust, of which by far the greatest contribution is from gas—commonly the very hot, X-ray emitting gas inhabiting galactic clusters, as discussed below. Certainly, MACHOs make only a trivial contribution to the energy density of dark matter. We now discuss some of the various candidates which have been proposed to constitute dark matter, as well as the experimental methods employed to search for them.

7.7 Baryonic dark matter

What is the nature of the dark matter which has been postulated to account for the phenomena described above? Some of the dark matter *must* be baryonic, since the value $\Omega_{\text{baryon}} \approx 0.04$ deduced from nucleosynthesis in the Big Bang is almost an order of magnitude larger than the closure parameter associated with visible stars, gas, and dust, of $\Omega_{\text{lum}} \sim 0.01$—see (5.31). In our own galaxy, some at least of this non-luminous baryonic dark matter has been accounted for in the form of compact halo objects (MACHOs) described above. However, X-ray studies of galaxy clusters reveal vast amounts of gas present between the galaxies in such clusters, and it seems possible that this accounts for almost half of the baryonic matter in the universe. Recent observations with the Chandra X-ray satellite, of absorption lines of oxygen and nitrogen, suggest that the other sources of the missing baryons are long filaments of gas associated with blazars (see Sections 9.10 and 9.14), which are AGN sources of TeV γ-rays.

There are no indications at present that more exotic baryonic objects such as mini black holes contribute significantly to the baryonic energy density. On the contrary, any primordial mini black holes of $M < 10^{11}$kg would have lifetimes less than the age of the universe, and in evaporating would emit Hawking radiation (as γ-rays)—see Sections 10.11 and 10.12. From the observed flux of γ-radiation from all sources one can set an upper limit on the energy density of such black holes of $\Omega_{\text{BH}} < 10^{-7}$.

In summary, baryonic matter makes only a small contribution to the overall density of the universe, and certainly less than 15% of the total estimated density of dark matter.

9.21 Detection of gravitational waves

When gravitational waves impinge on a detector, the difference in the acceleration from different parts of the wave can induce a deformation or strain, corresponding to an extension Δx in length x. The strain $h = \Delta x/x$ is given by

$$h^2 \sim \mathrm{G}\frac{P}{c^3\omega^2R^2} \tag{9.36}$$

where P is the power emitted by the source, R is its distance from the detector, and ω is the frequency of the radiation. Clearly, a detector with a quadrupole moment is necessary to excite a quadrupole amplitude. Inserting the value of P from (9.28) we find for the amplitude

$$h \sim \frac{GML^2\omega^2}{c^4R} \tag{9.37}$$

where the product $ML^2\omega^2$ is the second derivative of the quadrupole moment ML^2 of the source and is equal to the kinetic energy $E_{\mathrm{kin}} \sim Mv^2$ associated with the source oscillations. In a violent event such as the collapse to a neutron star, gravitational energy released due to the infall is of order $0.1\,M_{\mathrm{sun}}c^2$ (see Section 10.10). If we optimistically assume that 10% of this appears in the form of gravity waves then

$$h \sim \frac{GM_{\mathrm{sun}}}{100\,c^2R} \sim \frac{10^{-15}}{R} \tag{9.38}$$

where R is the distance of the source in parsec. For the local galaxy, $R \sim 10$ kpc and $h \sim 10^{-19}$, while for the Virgo cluster of galaxies $R \sim 10$ Mpc and $h \sim 10^{-22}$. Note that, even for a bar 1 km long, $h = 10^{-19}$ corresponds to a change in length of 10^{-16} m or one-tenth of a nuclear radius! It is likely that, by going further afield, the decrease in h with increasing R in (9.38) may be compensated by the R^3 increase in the number of sources and the possibility of much more violent events, such as collapse to massive black holes (AGNs), with gravitational wave energy far exceeding the solar mass energy.

Although the conceivable distortions to be measured by gravitational wave detectors as a result of the most violent cosmic events will be, at best, of order 10^{-20}, they are not considered to be beyond reach. The technique for their detection is based on split laser beams and a Michelson interferometer—see Fig. 9.29. The laser light is split into two paths at right angles by the beam splitter B. The beams are reflected back and forth by mirrors M1 – M4 (M1 and M3 being half-silvered) attached to masses and the fringes observed when the light beams recombine and interfere. A gravitational wave will effectively stretch one dimension, say $D1$, and contract the orthogonal dimension $D2$, thus causing a

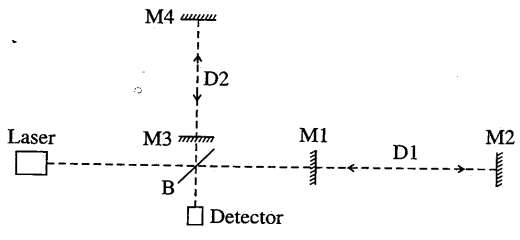

Fig. 9.29 Sketch of a Michelson interfe meter layout for a gravitational wave detec

fringe shift; alternatively, one can think of the gravitational wave as distorting the space/time between the mirrors, thus introducing tiny (Shapiro) delays in the relative transit times of the light beams. A Fabry-Perot etalon is used so that the beams make many traverses to and fro before recombining. As an example, the values chosen for the two LIGO experiments in the USA are $D1, D2 \sim 4\,\text{km}$, operating in a frequency range 10–1000 Hz, typical of the collapse times for neutron stars/black holes. In Europe, the dimensions of the VIRGO experiment are similar, while GEO600 is a smaller array with $L = 0.6\,\text{km}$. All of these experiments have very comparable sensitivities, and all are extremely difficult, and require years of tuning before scientific runs can commence.

The main problems for these experiments are the effects of background (seismic) noise, which kills all hope of detecting a signal below about 10 Hz. The noise problem can be tackled to some extent by combining the signals from two or more of the several detectors located in different positions worldwide, using timing information to reduce the noise and also indicate the direction of the source. For example, one of the LIGO and the TAMA (Japan) detectors have operated in coincidence for almost 500 h and placed an upper limit on any signal of < 0.12 events per day (Abbott *et al.* 2006). The feasibility of combining signals from all five of the above detectors has been proven, and serious scientific runs are commencing. More ambitious plans, aimed at avoiding low frequency (seismic) noise, are to place several gravity wave detectors in Earth orbit (codenamed LISA). There is no question that, with incremental improvements in the detection systems, gravitational waves will eventually be detected.

9.22 Summary

- The charged primary cosmic rays consist principally of high-energy nuclei of the elements, their chemical composition being in general similar to the solar system abundances. The exception is for lithium, beryllium, and boron, which are abundant in the cosmic rays and produced by spallation of heavier nuclei in collisions with interstellar matter.
- The energy spectrum up to 10^{15} eV falls off as a power law, $\mathrm{d}N/\mathrm{d}E \sim E^{-2.7}$, and decreases more rapidly at higher energy, up to at least 10^{20} eV.
- The charged primary radiation is affected by Solar System magnetic fields. The Earth's field imposes a cut-off in momentum depending on magnetic latitude. Cosmic rays are also moderated by solar effects (the solar wind) which follows the 11-year sunspot cycle.
- The energy density in cosmic rays, at about $1\,\text{eV}\,\text{cm}^{-3}$, is comparable with that in the cosmic microwave background, in starlight and in galactic magnetic fields. The rate at which energy needs to be injected into the cosmic rays can be accounted for in terms of shock-wave acceleration in supernova shells, provided these processes have efficiencies of a few percent. While this mechanism can work up to energies of 10^{14} eV, the acceleration mechanism for the highest energies is unknown.
- The cosmic rays at sea-level are of secondary origin, and generated by collisions of the primaries in the atmosphere. The hard component consists of muons from decay of charged pions created in the atmosphere,